International Conference on Space Optics—ICSO 2024
Antibes Juan-les-Pins, France
21-25 October 2024

Edited by Philippe Kubik, Frédéric Bernard, Kyriaki Minoglou and Nikos Karafolas

PLATO Flight Model Cameras TVAC focus calibration

International Conference on Space Optics — ICSO 2024, edited by Frédéric Bernard, Nikos Karafolas, Philippe Kubik, Kyriaki Minoglou, Proc. of SPIE Vol. 13699, 1369965 · © 2025 ESA and CNES · 0277-786X · doi: 10.1117/12.3071286

PLATO Flight Model Cameras TVAC focus calibration

Martin Pertenais[a], Philipp Eigmüller[b], Juan Cabrera[b], Denis Grießbach[a], Tim A. van Kempen[c], Lorenza Ferrari[d], Wouter Laauwen[d], Thierry Appourchaux[e], Cydalise Dumesnil[e], Véronique Hervier[e], Nicolas Beraud[e], Pierre Guiot[e], Vincent Hamm[e], Mathieu Condamin[e], Serge François[e], Catherine Tamiatto[e], Pierre-Amaury Westphal[e], Gonzalo Ramos Zapata[f], Francisco Montoro[f], Elisa Borreguero[f], Mª Teresa Rodrigo[f], Ángel L. Valverde[f], Mª Ángeles Sierra[f], Lucía Espinosa[f], Amaia Santiago[f], Fernando Conde[f], Nicolas Gorius[g], Claudio Arena[g], Francesco Borsa[h], Alessio Aboudan[i], Rik Huygen[j], Sara Regibo[j], Pierre Royer[j], Bart Vandenbussche[j], Aline Hermans[k], Ann Baeke[k], Miguel Mas-Hesse[l], and Heike Rauer[b,m]

[a]Institute of Optical Sensor Systems, German Aerospace Center (DLR), Rutherfordstr. 2, 12489 Berlin, Germany
[b]Institute of Planetary Research, German Aerospace Center (DLR), Rutherfordstr. 2, 12489 Berlin, Germany
[c]SRON Netherlands Institute for Space Research Leiden, Niels Bohrweg 4, 2333-CA, Leiden, the Netherlands
[d]SRON Netherlands Institute for Space Research, Landleven 12, 9747 AD Groningen, The Netherlands
[e]IAS, Institut d'Astrophysique Spatiale, UMR8617, 91405 Orsay, France
[f]INTA - Instituto Nacional de Técnica Aeroespacial, Ctra. Ajalvir, Km 4, 28850 Torrejón de Ardoz, Spain
[g]INAF - Osservatorio Astrofisico di Catania, Italy
[h]INAF - Osservatorio Astronomico di Brera, Via E. Bianchi 46, 23807 Merate (LC), Italy
[i]CISAS G. Colombo - University of Padova, Italy
[j]Institute of Astronomy, KU Leuven, Celestijnenlaan 200D, bus 2401, 3001 Leuven, Belgium
[k]Centre Spatial de Liège (CSL), Av. du Pré Aily, 4031 Liège, Belgium
[l]Centro de Astrobiologia (CSIC-INTA), 28850 Torrejon de Ardoz, Madrid, Spain
[m]Institut für Geologische Wissenschaften, Freie Universität Berlin, Malteserstraße 74-100, 12249 Berlin, Germany

ABSTRACT

The PLAnetary Transits and Oscillations of stars (PLATO) mission aims at detecting and characterizing extrasolar planetary systems, including terrestrial exoplanets orbiting up to the habitable zone around bright solar-type stars[1,2]. The scientific payload of PLATO, developed and provided by the PLATO Mission Consortium (PMC) and ESA, is based on a multi-telescope configuration consisting of 24 Normal Cameras (N-CAM) and 2 Fast Cameras (F-CAM), so as to provide simultaneously a large field of view and a large collecting aperture. Each individual camera can be thermally re-focused in order to compensate for the accumulated integration errors between the Telescope Optical Unit (TOU) and the Focal Plane Assembly (FPA). It allows to operate each camera in-orbit at its optimum setpoint, minimizing the average PSF size of the stars on the focal plane. To achieve this, the camera itself is cold-biased on the spacecraft and its temperature is controlled by a Thermal Control System (TCS) that allows to reach a commanded stable temperature within the range [-90°C ; -70°C]. This work presents the preparation and results of the on-ground pre-launch calibration campaign of the cameras Flight Models (FM), scanning the complete temperature range and searching for the best focus temperature. A

Further author information: martin.pertenais@dlr.de

set of statistical data is presented, based on the assembly and testing of the first flight model cameras, confirming their high-quality and validating the processes defined for the serial production.

Keywords: PLATO, exoplanet, Camera, Focus, Calibration, TVAC, AIT

1. INTRODUCTION AND CONTEXT

1.1 PLATO Payload and Camera Description

The PLATO payload is made of 24 identical "normal" cameras (N-CAM), 2 "fast" cameras (F-CAM), and a Data Processing System (DPS).

As detailed in Ref. 3, the 24 N-CAMs are split into 4 groups of 6 on the Spacecraft (S/C), each group being tilted by 9.2° away from the S/C Z axis (equal to the F-CAM Boresight). This allows to increase considerably the total field of view of PLATO without impacting too much the noise budget by keeping several cameras pointing to the same stars, see Ref. 4. These 26 cameras will be used to constantly acquire stable images of thousands of star simultaneously during 4 years. By plotting the integrated flux of each star Point Spread Function (PSF) over time, photometric time-series of each star can be created to evaluate the photometric variation of the star. In case of an exoplanet transit, this time-series will show a typical transit shaped drop of the integrated flux allowing the scientists to compute several parameters of the star-planet couple, such as relative size of the planet, orbit duration, orbit inclination. In combination with the asteroseismology measurements of the star itself, the age of the system and the mass of the star can also be determined.

Each camera is composed by a Telescope Optical Unit (TOU),[5] a Focal Plane Assembly (FPA)[6] and a Front End Electronic unit (FEE). Figure 1 shows a picture of one flight model camera after integration at the Centre Spatial de Liège (CSL) in Belgium. A Data Processing Unit (DPU) gathers the data of 2 cameras simultaneously before transferring it to the Instrument Control Unit (ICU) that packetize and compress the data of the complete Payload before sending it to ground via the Spacecraft.

Figure 1. Picture of camera FM22 at CSL after integration of the TOU with its analogue chain (FPA+FEE),

1.2 Camera Focus Calibration Concept

As described in Ref. 3, PLATO's cameras have the uncommon feature of thermal refocusing capability. While each camera is designed to be mechanically athermal, the optical design[7] has been performed such as to offer

optical thermal refocusing. The temperature of each camera is controlled by heaters placed on its tube near the optical pupil. These heaters are used to regulate the camera temperature to very stable levels. By tuning these temperature heaters, a linear change of at least 10 µm/K is expected on the optical focus of the camera.This will be used in-orbit to refocus each camera individually to its optimum focus temperature maximizing the Signal to Noise Ratio (SNR).[8]

Knowing that the cameras are designed to meet all their performance requirements at -80°C ±10°C, the total available focusing range available is of ±100 µm. This focusing range has to be broken down into several contributors for each of the units and sub-systems involved in the camera, to then verify that the expected defocus is well within this range. The full focus end-to-end process is as follows:

- Determination of the TOU best image plane position at -80°C, described in Ref. 9
- Determination of the FPA mean sensitive area position, described in Ref. 6
- Computation of the bolting position at ambient temperature to match the 2 previous positions at -80°C, described in Ref. 10
- Bolting of the TOU to the FPA at ambient, described in Ref. 11
- Optical focus calibration in TVAC around -80°C at the test houses, described in this paper.

The goal of the camera best focus search calibration[12] is to determine the optimal operational temperature of every individual camera. The accumulation of uncertainties and tolerances on the integration and measurement sequence described above leads to a focus error in theory of up to 72µm.[3] These +/-72µm could be compensated by a temperature change of the camera of +/-6K, using 12µm/K sensitivity (current best estimate). We expect on top of that, a change of best focus temperature in-orbit compared to the ground measured of up to +/-2K. This is mostly due to thermal environment difference, OGSE performance vs stars, launch and Thermo-Elelastic Distortion (TED) effects.

The global concept of this camera focus calibration, described in more details in the following chapter, is to illuminate the camera with a set of point-source across the complete field of view and estimate the optical quality of the camera (through the average PSF size in the FoV). This is repeated for a set of 5 temperatures: -90°C, -85°C, -80°C, -75°C, and -70°C to finally fit our merit function of average PSF size versus camera temperature and determine the best focus temperature of that particular camera. Note the 2 F-CAMs are treated similarly to the N-CAMs here, as we don't expect any relevant difference in terms of best focus calibration.

1.3 Test Houses Setup

To achieve this optical calibration, and after integration in one of the both CSL1 or CSL2 lines at CSL in Belgium, each camera flight model will visit one of the three available test houses for the project: IAS in Orsay (France), INTA in Madrid (Spain) or SRON in Groningen (Netherlands). An almost identical setup was designed, developed and implemented at these 3 facilities to allow for a comparable calibration results.

The setup is composed by an optical collimator designed for the purpose at University of Lisbon[13] and common to all 3 Test Houses. This stable white light point-source collimator illuminates the entrance pupil of the camera, placed inside a TVAC chamber. Note that at SRON the collimator is placed inside the chamber as shown in Fig. 2, while it remains outside at IAS and INTA. To be able to reach its complete field of the view, the camera is placed either on an hexapod (at IAS) or inside a gimbal (at SRON and INTA), as seen in Fig. 3. A thermal environment box was created around the camera in order to replicate as accurately as possible the expected temperature environment during environment.

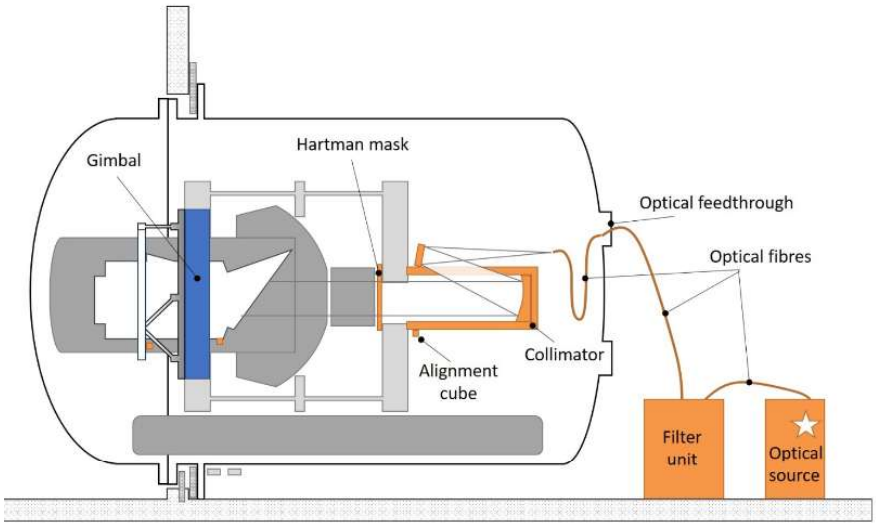

Figure 2. Test Setup schematics at SRON.

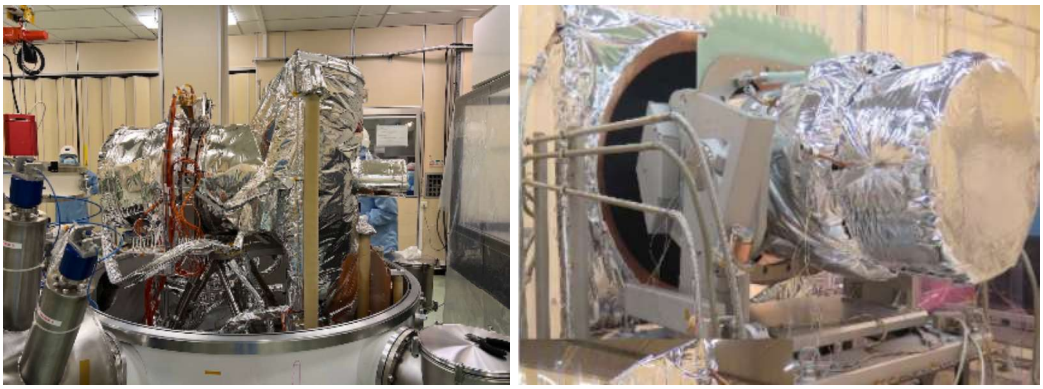

Figure 3. Picture of an FM camera installed on the hexapod inside its thermal environment box before closure of the TVAC chamber at IAS on the left, and another one in the gimbal at INTA on the picture on the right. SRON setup not shown for better figure visibility.

2. INDIVIDUAL CAMERA FOCUS CALIBRATION

2.1 Commanding and analysis parameters

All the cameras follow the same calibration procedure that goes as follow for each of the 5 temperatures points:

- Point the Camera to FoV point number 1
- Acquire 2 background frames with the OGSE shutter closed
- Acquire 5 frames with the OGSE shutter open
- Move randomly the camera by the angular equivalent of a fraction of a pixel
- Acquire 5 frames, and repeat 25 times this dithering
- Move to the next FoV position and repeat for all 40 FoV positions.

The 40 field of view positions visited were chosen such that each of them cover the same field of view area. As PLATO cameras will observe a tremendous number of starts simultaneously, each FoV point has the same

scientific importance, a priori. This list of field of view positions was initially defined for the testing of the EM camera.[14]

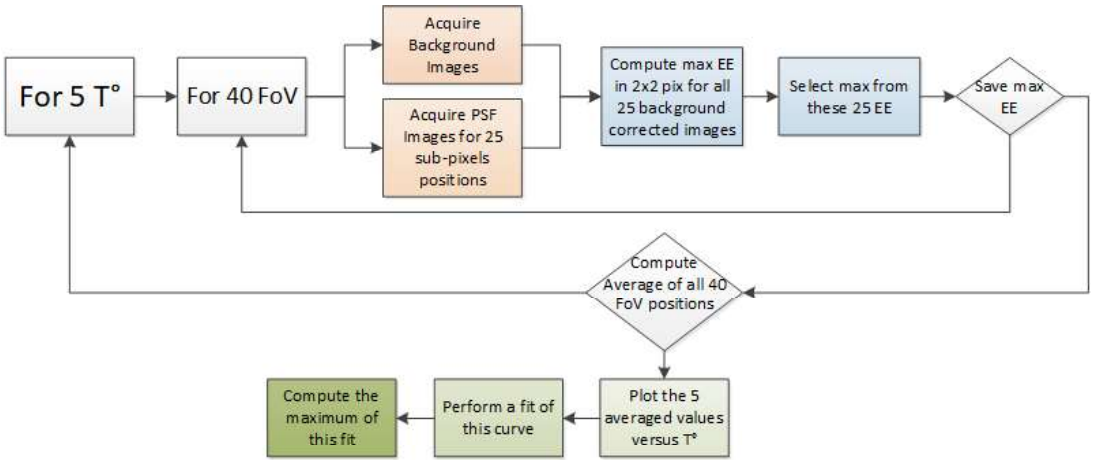

Figure 4. Logical flow of commanding and analysis of the best focus calibration of a camera

As described in Ref. 14, the merit function to determine the PSF size at each FoV position is the Ensquared Energy Fraction (EEF) in 2x2 pixels. This simple metric is computed by comparing the amount of energy (photo-electrons, or digital numbers in practice) inside the brightest 2x2 pixels square of the PSF to the total amount of energy in the normalization square, of at least 7x7 pixels. If the PSF is very sharp and fully contained within 2x2 pixels, the EEF would then be 100%. The higher the EEF, the sharper the PSF.

Figure 4 shows the concept of the commanding and analysis best focus calibration for each camera. The 25 sub-pixels positions commanded are necessary in order to remove a major contributor of the PSF size: the so-called phase function of optical PSF on the detector pixel grid. By projecting an optical PSF onto a pixel grid, it becomes clear that the sub-pixel position of the centroid of the PSF on the grid has a direct and significant impact on the measured EEF. Simulations have shown that, by performing this dithering and acquiring the same optical PSF at 25 random positions on the pixel grid (we assume that the optical PSF is locally the same), we can get rid of this uncertainty and have a consistent and repeatable method.

2.2 Example of one camera FM results

One of the flight model camera (FM12) already tested is used here as example to show the analysis steps and results obtained. The plots and conclusions shown here, are of course produced for all the individual cameras. Section 3 below will give more insights in the comparison and statistics of all the tested models up to date.

Figure 5 shows the output of the analysis script for all the 5 temperatures measured with camera FM12. For each temperature, the Ensquared Energy Fraction in 2x2 pixels is plotted as a function of the FoV position. In the top row, the EEF value is encoded in the circle size (the bigger the circle, the bigger the PSF), while an interpolated color map is plotted in the bottom row.

The first conclusion looking at these results is that the thermal focusing concept of the camera works! For each temperature set-point, we observe a significantly different optical quality of the camera with bigger or sharper PSFs across the FoV. It also clear that the actual best focus temperature for this camera appears to be very close to the nominal value of -80°C. Finally, another observation is the spatial dependence of the focus. The four inner positions of the FoV, close to the optical axis, appear to have a significantly different best focus temperature (closer to -85°C) than the remaining positions of the FoV. This is caused by the field curvature aberration of the TOU, and was expected per analysis.

The next step of the analysis is to average these 40 values for each temperature point and perform a polynomial fit of the 5 points, to determine the best focus temperature of that camera. The result is shown in Fig. 6. Two different kind of functions were fitted for comparison: a Gaussian function and a 4th order polynomial function. Both provide very similar results with a best focus temperature of -79.5°C.

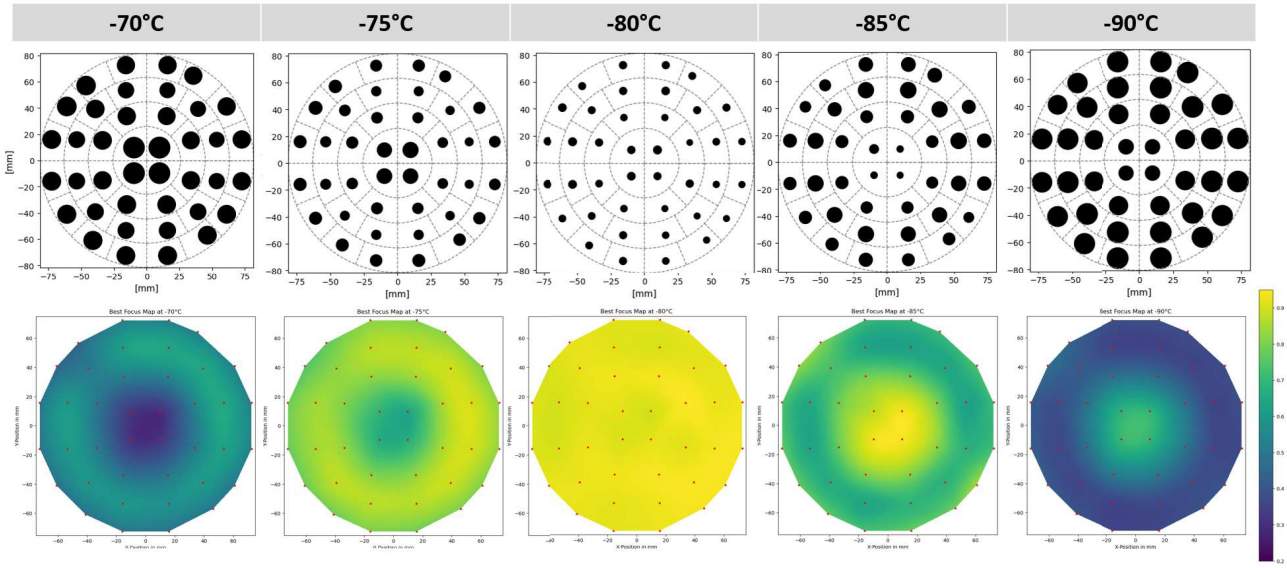

Figure 5. Ensquared Energy Fraction in 2x2 pixels for camera FM12, plotted as a function of the FoV position. In the top row, the EEF value is encoded in the circle size, while an interpolated colormap is plotted in the bottom row.

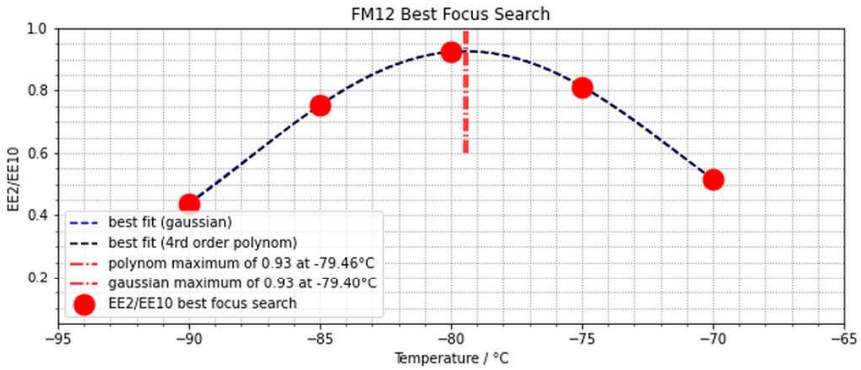

Figure 6. Best Focus Temperature fit for camera FM12

3. RESULTS COMPARISON FOR ALL TESTED CAMERAS

3.1 Camera Engineering Model (EM)

As described in Ref. 14, the camera Engineering Model was used to validate each of the 3 test houses setup independently. It was tested and calibrated in all the 3 setups following the same procedure. This work helped understanding the systematics due to the setups and better apprehend the error bars of the best focus temperature (BFT) determination.

A BFT of -74.0°C was measured at IAS, -77.6°C at SRON, and finally -75.7°C at INTA. Assuming that the camera didn't change between the 3 measurements, this total of 3.6K spread of the results provide a good first estimate of the uncertainties due to the setup themselves. From that point, it was decided to consider systematics of $\pm$ 2°C on the computed BFTs. The data analysis was performed by at least 3 different analysts, all using an independent analysis script. Results were in all the case within 0.2°C precision. This means that the analysis of the data itself is very precise, and that the error bar is driven by the acquisition of the data, hence the setup itself. With that in mind, and assuming again that the camera EM didn't change during the 3 measurements, the difference in BFT measured at the 3 test houses can be defined as a systematic offset.

With INTA providing a BFT between IAS and SRON, it is considered as the reference for this offset computation. IAS would then have an offset of +1.7°C compared to INTA, and SRON an offset of -1.9°C compared to INTA.

3.2 Flight Models

At the time of writing, a total 19 flight model cameras were completed tested and calibrated. from these 19, 3 of them unfortunately couldn't follow the nominal best focus temperature calibration for schedule reasons. An alternative method demonstrated that using transient measurements during cool-down and warm-up measurement, the BFT could be estimated with sufficient accuracy. This method is not presented in this paper, where we will focus on the other 16 tested flight cameras.

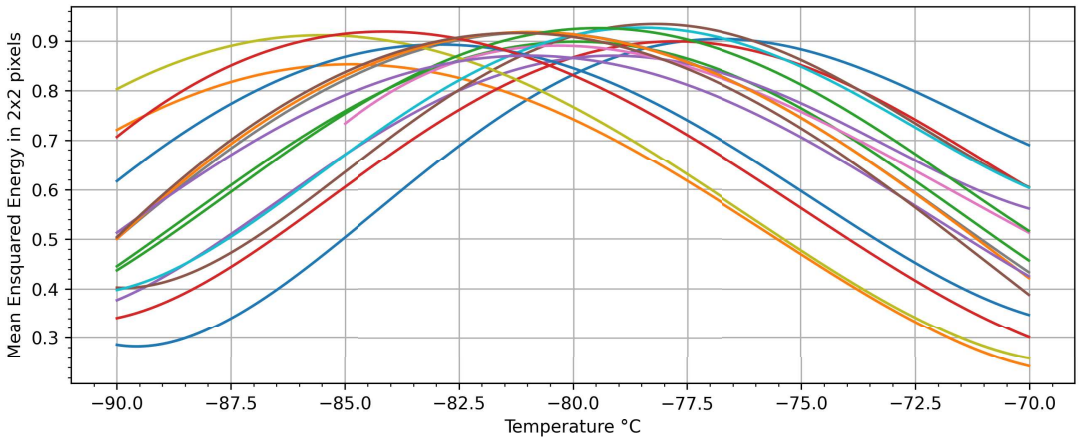

Figure 7. Overlap of the 16 fitted best focus temperature curves for the camera flight models.

Figure 7 shows an overlap of the 16 fitted best focus temperature curves. The ± 6°C expected range of uncertainty described in Section 1 is thereby confirmed with maxima of the curves ranging from -85.5°C to -76.5°C. This overlap plot also provides evidence that all the cameras appear to behave in a very similar way across temperature around their own BFT. In order to verify this statement, these 16 curves where all centered on their own BFT, and the 5×16 measured EEF points where plotted on top of each other. The result is shown in Fig. 8.

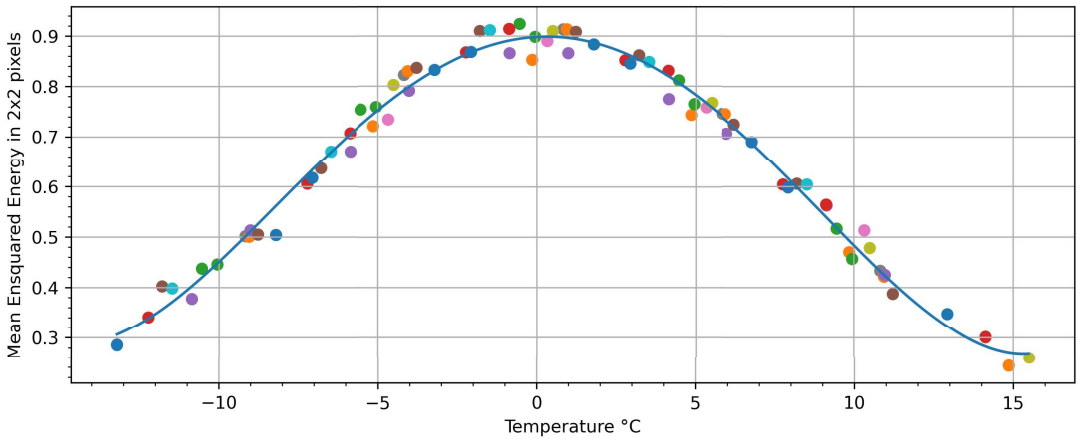

Figure 8. Overlap of the 5*16 measured EEF points (uncorrected values), centered on their own BFT. Each color represents the 5 temperature measurement points of an individual camera.

Based on this new data set of 5×16 points, a new polynomial fit was performed to determine a common function applicable to all the cameras. These are the corresponding polynomial coefficients: [1.25 10^{-5}; -1.9 10^{-5}; -5.5 10^{-3}; 3.6 10^{-3}; 0.9]. Thanks to this function, we can now anticipate the complete response of a camera by having only 1 or 2 temperature points at our disposal. This plot is also really helpful to flag any potential outlier camera, that wouldn't behave like the previous one.

Even if 19 cameras (+ the EM) remains a relatively small number, some statistics are presented below. Figure 9 shows the overview of all the BFTs computed so far. The color code corresponds to which test house actually calibrated that particular camera.

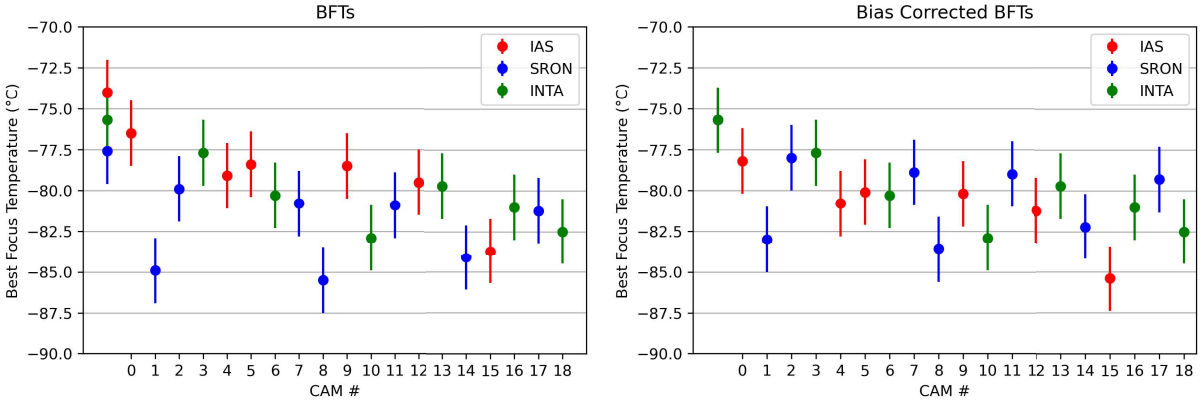

Figure 9. Overview plots of the 16 BFTs measured so far, on top of the EM camera (id -1). The offsets from the EM values were corrected on the figure on the right for the SRON and IAS data points.

The camera with id=-1 in the X axis of the plots corresponds to the EM mentioned in the previous chapter, hence the 3 points for the same camera. In the right hand side figure, the offsets computed in Section 3.1 were applied as correction factor to the other cameras tested at IAS and SRON. Similarly, the histogram of the distribution of these 16 points is presented in Fig. 10. All the relevant average, median and standard deviation for several camera combination are presented in Table 1.

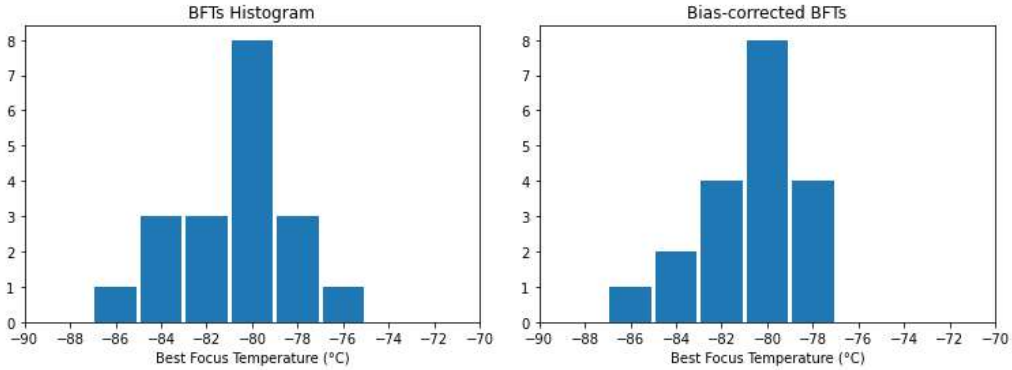

Figure 10. Histogram of the distribution of the 19 measured BFTs, with and without EM correction factors

As seen in the individual fits above, these figures and table confirm the compliance of all the cameras tested up to now. Independently from the EM correction application or not, all the cameras showcase a best focus temperature well within the [-90°C;-70°C] range. The expected alignment uncertainty of ± 6 K is also well respected. The distribution seen in the histograms in Fig. 10, shows that almost half of the tested camera have a BFT of -80°C ± 1°C, confirming the validity of the whole integration process, from the TOU and FPA to the alignment at CSL. It seems that the distribution is however slightly cold biased, with a mean BFT of -80.9°C

(and -80.7°C for the EM corrected distribution). Until the cameras are in-orbit and re-calibrated in their real environment with stars, it is impossible to identify the root cause for this bias. It could be due to the collimator design, the thermal environment, or a real bias in the integration concept.

Table 1. Mean, Median and standard deviation value of the BFT (°C) for several combinations.

	Raw		EM Corrected		
	Mean	Median	Mean	Median	STD
CSL1	-79.7	-79.8	-79.7	-79.2	2.0
CSL2	-82.2	-82.5	-82.0	-82.2	2.2*
INTA	-80.7	-80.7	-80.7	-80.7	1.7
IAS	-79.3	-78.8	-81.0	-80.5	2.2
SRON	-82.5	-81.2	-80.6	-79.3	2.1
all	-80.9	-80.8	-80.7	-80.3	2.0

*1.1°C for the corrected

The numbers in Table 1 provide many insights in the dependencies and differences between the 3 test houses, but also the 2 integration lines used at CSL to assemble to the TOUs to the FPAs. In all the different cases, the standard deviation of the distributions remain around 2°C ± 0.3°C, except for the EM corrected case of the CSL2 integration line with 1.1°C.

On the test houses differences, the EM correction factors described above appear to provide excellent results, with a mean BFT for the 3 test houses after correction of -80.7°C, -80.5°C and -80.6°C for respectively INTA, IAS and SRON. A larger discrepancy is found between the 2 integration lines at CSL with average BFTs of respectively -79.7°C and -82.0°C after application of the EM correction factor. Investigations are still on-going to find the root cause of this bias between the 2 identical lines at CSL.

4. CONCLUSIONS AND NEXT STEPS

This paper provided an overview of the focus calibration concept for the flight model cameras of the PLATO Payload, planned for launch in December 2026.

The setup created at the 3 test houses, after validation with the camera engineering model, is now a great platform for the verification, characterization and calibration of the flight models. A total of 19 flight models have now been fully tested at the time of writing, with 16 of them following the full focus calibration process. We presented the commanding and analysis process for the focus calibration, where a change of the camera temperature (through heaters and a Thermal Control System algorithm) allows us to compensate for the mechanical defocus introduced during the alignment process. This mechanical defocus is the result of a stack of uncertainties and tolerances across the integration process of the camera.

While some differences are observed between the 3 test houses, and between the 2 integration lines at CSL, the overall distribution of the 19 tested camera provide a great validation of our focusing budget and test setup. The average BFT for these 19 cameras, after correction of the offsets between the 3 test houses determined with the camera EM, is -80.7°C, with a standard deviation of 2°C. A total of 7 flight cameras are still to be calibrated before delivery to the S/C, including the 2 F-CAMs for which we expect no relevant difference in terms of best focus calibration.. The next step will then be to re-calibrate the best focus temperature of the cameras in space, during the commissioning of the Payload. This will be done using a distribution of stars in the field of view, and using the BFT determined on ground as input. This final calibration will ensure that each individual camera is operated in such a way to maximize its scientific return.

ACKNOWLEDGMENTS

This work presents results from the European Space Agency (ESA) space mission PLATO. The PLATO payload, the PLATO Ground Segment and PLATO data processing are joint developments of ESA and the PLATO Mission Consortium (PMC). Funding for the PMC is provided at national levels, in particular by countries participating

in the PLATO Multilateral Agreement (Austria, Belgium, Czech Republic, Denmark, France, Germany, Italy, Netherlands, Portugal, Spain, Sweden, Switzerland, Norway, and United Kingdom) and institutions from Brazil. The authors thank the Belgian Federal Science Policy Office (BELSPO) for the provision of financial support in the framework of the PRODEX Programme of the European Space Agency (ESA) under contract number PEA 4000137604. IAS gratefully acknowledge financial support by CNES. M.A. acknowledges support from the German Aerospace Center (DLR FKZ 50OP1902). Members of the PLATO Consortium can be found at https://platomission.com/. The ESA PLATO mission website is https://www.cosmos.esa.int/plato. We thank the teams working for PLATO for all their work.

REFERENCES

[1] Rauer, H., Aerts, C., Cabrera, J., Deleuil, M., Erikson, A., Gizon, L., Goupil, M., Heras, A., Lorenzo-Alvarez, J., Marliani, F., Martin-Garcia, C., Mas-Hesse, J. M., O'Rourke, L., Osborn, H., Pagano, I., Piotto, G., Pollacco, D., and et al., "The PLATO Mission," *arXiv e-prints* , arXiv:2406.05447 (June 2024).

[2] Rauer, H., Catala, C., Aerts, C., Appourchaux, T., Benz, W., Brandeker, A., Christensen-Dalsgaard, J., Deleuil, M., Gizon, L., Goupil, M.-J., and et al., "The PLATO 2.0 mission," *Experimental Astronomy* **38**, 249–330 (Sep 2014).

[3] Pertenais, M., Cabrera, J., Paproth, C., Boerner, A., Griessbach, D., Mogulsky, V., and Rauer, H., "The unique field-of-view and focusing budgets of PLATO," in [*International Conference on Space Optics — ICSO 2020*], Cugny, B., Sodnik, Z., and Karafolas, N., eds., **11852**, 2043 – 2054, International Society for Optics and Photonics, SPIE (2021).

[4] Ragazzoni, R., Magrin, D., Rauer, H., Pagano, I., Nascimbeni, V., Piotto, G., Piazza, D., Levacher, P., Schweitzer, M., Basso, S., Bandy, T., Benz, W., Bergomi, M., Biondi, F., Boerner, A., Borsa, F., Brandeker, A., Brändli, M., Bruno, G., Cabrera, J., Chinellato, S., Roche, T. D., Dima, M., Erikson, A., Farinato, J., Munari, M., Ghigo, M., Greggio, D., Gullieuszik, M., Klebor, M., Marafatto, L., Mogulsky, V., Peter, G., Rieder, M., Sicilia, D., Spiga, D., Viotto, V., Wieser, M., Heras, A. M., Gondoin, P., Bodin, P., and Catala, C., "PLATO: a multiple telescope spacecraft for exo-planets hunting," in [*Space Telescopes and Instrumentation 2016: Optical, Infrared, and Millimeter Wave*], MacEwen, H. A., Fazio, G. G., Lystrup, M., Batalha, N., Siegler, N., and Tong, E. C., eds., **9904**, 731 – 737, International Society for Optics and Photonics, SPIE (2016).

[5] Magrin, D., Munari, M., Pagano, I., Piazza, D., Ragazzoni, R., Arcidiacono, C., Basso, S., Dima, M., Farinato, J., Gambicorti, L., Gentile, G., Ghigo, M., Pace, E., Piotto, G., Scuderi, S., Viotto, V., Zima, W., and Catala, C., "PLATO: detailed design of the telescope optical units," in [*Space Telescopes and Instrumentation 2010: Optical, Infrared, and Millimeter Wave*], Jr., J. M. O., Clampin, M. C., and MacEwen, H. A., eds., **7731**, 715 – 722, International Society for Optics and Photonics, SPIE (2010).

[6] Moreno, J., Vielba, E., Manjón, A., Motos, A., Vázquez, E., Rodríguez, E., Saez, D., Sengl, M., Fernández, J., Campos, G., Muñoz, D., Mas, M., Balado, A., Ramos, G., Cerruti, C., Pajas, M., Catalán, I., Alcacera, M. A., Valverde, A., Pflueger, P., and Vera, I., "PLATO FPA. focal plane assembly of PLATO instrument," in [*International Conference on Space Optics; ICSO 2018*], *Society of Photo-Optical Instrumentation Engineers (SPIE) Conference Series* **11180**, 111803N (July 2019).

[7] Magrin, D., "PLATO telescope optical units: An update on working status," in [*Space Telescopes and Instrumentation 2020: Optical, Infrared, and Millimeter Wave*], *Society of Photo-Optical Instrumentation Engineers (SPIE) Conference Series* **11443-80** (2020).

[8] Börner, A., Paproth, C., Cabrera, J., Pertenais, M., Rauer, H., Mas-Hesse, J. M., Pagano, I., Alvarez, J. L., Erikson, A., Grießbach, D., Levillain, Y., Magrin, D., Mogulsky, V., Niemi, S.-M., Prod'homme, T., Regibo, S., De Ridder, J., Rockstein, S., Samadi, R., Serrano-Velarde, D., Smith, A., Verhoeve, P., and Walton, D., "PLATO's signal and noise budget," *Experimental Astronomy* **58**, 1 (Aug. 2024).

[9] Novi, A., Battistelli, E., Burresi, M., Capuano, E., Dami, M., Marinai, M., Postiglione, G., Taiti, M., Farinato, J., Magrin, D., and Pagano, I., "An industrialized and deterministic approach for aligning and focusing the 26 PLATO refractive telescopes, designed for operating in space," in [*Space Telescopes and Instrumentation 2022: Optical, Infrared, and Millimeter Wave*], Coyle, L. E., Matsuura, S., and Perrin, M. D., eds., **12180**, 121804L, International Society for Optics and Photonics, SPIE (2022).

[10] Royer, P., Baeke, A., Terrasa, G., Huygen, R., Regibo, S., Farinato, J., Magrin, D., Mazzoli, A., Pajas, M., Vandenbussche, B., Hermans, A., Millou, G., Vassallo, D., Margeli, A. B. B., Clermont, L., Cottinelli, A., Ferrari, L., Gorius, N., Laauwen, W., Levillain, Y., Novi, A., Pagano, I., Pertenais, M., Zapata, G. R., Salatti, M., and Kempen, T. A. V., "Alignment and integration of the first PLATO camera," in [*Space Telescopes and Instrumentation 2022: Optical, Infrared, and Millimeter Wave*], Coyle, L. E., Matsuura, S., and Perrin, M. D., eds., **12180**, 121804H, International Society for Optics and Photonics, SPIE (2022).

[11] Royer, P., L. Clermont, J., M. Pertenais, A. Baeke, Huygen, R., J. De Ridder, Regibo, S., M. Dami, Vandenbussche, B., A. Belen Balado Margeli, J. Farinato, D. Greggio, Y. Levillain, D. Magrin, L. Marafatto, M. Pajas, G. Ramos Zapata, A.L. Valverde Guijarro, and V. Viotto, "On the optical alignment of the PLATO cameras," in [*Space Telescopes and Instrumentation 2020: Optical, Infrared, and Millimeter Wave*], *Society of Photo-Optical Instrumentation Engineers (SPIE) Conference Series* **11443**, 111443L (Aug. 2020).

[12] Pertenais, M., Cabrera, J., Griessbach, D., Erikson, A., Vandenbussche, B., Samadi, R., Reese, D., and Rauer, H., "Overview of PLATO's cameras on-ground and in-orbit calibration and characterisation," in [*International Conference on Space Optics — ICSO 2020*], Cugny, B., Sodnik, Z., and Karafolas, N., eds., **11852**, 1185209, International Society for Optics and Photonics, SPIE (2021).

[13] Abreu, M., Alves, D. C., Cabral, A., Coelho, J. M., Santos, P., Clermont, L., Baeke, A., and Vandenbussche, B., "A white light collimator for Plato camera integration support," in [*Space Telescopes and Instrumentation 2020: Optical, Infrared, and Millimeter Wave*], Lystrup, M., Perrin, M. D., Batalha, N., Siegler, N., and Tong, E. C., eds., **11443**, 114434T, International Society for Optics and Photonics, SPIE (2020).

[14] Borsa, F., Cottinelli, A., Gorius, N., Arena, C., Vandenbussche, B., Regibo, S., Huygen, R., Royer, P., Pertenais, M., Martin, C., Appourchaux, T., Alvarez, J. L., van Kempen, T. A., Laauwen, W., Pagano, I., and Ragazzoni, R., "PLATO EM first cryogenic vacuum test campaign PSF results," in [*Space Telescopes and Instrumentation 2022: Optical, Infrared, and Millimeter Wave*], Coyle, L. E., Matsuura, S., and Perrin, M. D., eds., **12180**, 121801D, International Society for Optics and Photonics, SPIE (2022).